



# Debris flows in the Lushan earthquake area: formation characteristics, rainfall conditions, and evolutionary tendency

Xiaojun Guo<sup>1,2</sup> · Xingchang Chen<sup>3</sup> · Guohu Song<sup>4</sup> · Jianqi Zhuang<sup>5</sup> · Jianglin Fan<sup>6</sup>

Received: 15 May 2020 / Accepted: 19 January 2021 / Published online: 2 February 2021  
© The Author(s), under exclusive licence to Springer Nature B.V. part of Springer Nature 2021

## Abstract

Debris flows often occur in the mountainous watersheds of earthquake-affected areas, and in the Lushan earthquake area of southwestern China, they have become a significant hazard. In this study, the influencing factors and spatial distribution of debris flows were analyzed through a review of their occurrence history. Debris flows are mainly distributed in the northwestern part of the study area, which hosts the greatest density of active faults. The debris flows are generally formed by the ‘progressive bulking’ effect in channels, and deep incision, lateral erosion, and blockage breaking are common processes that amplify the magnitude of such debris flows. Rainfall thresholds for different types of debris flow were proposed to explain the spatial differences between debris-flow regions, and the temporal variations of those thresholds highlighted how the rainfall conditions required for the occurrence of debris flows have changed. Natural vegetation recovery, reduction in the availability of solid material, and artificial debris-flow control projects play important roles in raising the threshold of the rainfall conditions required for triggering debris flows.

**Keywords** Debris flows · Formation mechanism · Rainfall thresholds · Spatial distribution · Lushan earthquake

---

✉ Xiaojun Guo  
aaronguo@imde.ac.cn

✉ Xingchang Chen  
chenxingchang@swust.edu.cn

<sup>1</sup> Key Laboratory of Mountain Hazards and Surface Process, Institute of Mountain Hazards and Environment, Chinese Academy of Sciences, Chengdu 610041, China

<sup>2</sup> CAS Center for Excellence in Tibetan Plateau Earth Sciences, Beijing 100101, China

<sup>3</sup> School of Environment and Resource, Southwest University of Science and Technology, Mianyang 621020, China

<sup>4</sup> Sichuan Institute of Geological Engineering Investigation Group Co. LTD, Chengdu 610032, China

<sup>5</sup> School of Geological Engineering and Surveying, Changan University, Xi’an 710064, China

<sup>6</sup> Sichuan Provincial Meteorological Observatory, Chengdu 610072, China

## 1 Introduction

The Longmenshan fault zone of southwestern China is located at the southeastern margin of the Tibetan Plateau and corresponds to a region of high seismic activity (Wang and Meng 2009; Chen et al. 2014). Two catastrophic earthquakes have struck this region in recent years: the Ms 8.0 Wenchuan earthquake (May 12 2008) and the Ms 7.0 Lushan earthquake (April 20 2013). Strong earthquakes commonly trigger slope failures in mountainous regions characterized by high relief and deeply incised valleys, and the material that accumulates in gully channels provides the main source for post-seismic debris flows (Cui et al. 2014; Guo et al. 2016a). In regions affected by earthquakes, the post-seismic debris-flow hazard can persist for decades, as exemplified by the debris flows associated with the occurrence of the Ms 7.6 Chichi earthquake in 1999 and the MS 8.0 Wenchuan earthquake in 2008 (Lin et al. 2003; Chen et al. 2005, 2016; Cui et al. 2014; Guo et al. 2016a).

It is important in an investigation of debris-flow activity to complete a debris-flow inventory and/or database, and to analyze the characteristics, distribution patterns, and controlling factors of such events. Previous studies of post-seismic debris flows have endeavored to investigate the factors that control their distribution (Yin et al. 2009; Cui et al. 2011; Chen et al. 2016; Guo et al. 2016b), their formation and development mechanisms (e.g., Cui et al. 2013; Ouyang et al. 2015; Guo et al. 2016c), possible rainfall thresholds (e.g., Shieh et al. 2009; Zhou et al. 2014; Guo et al. 2016b; Ma et al. 2017), and other environmental variables (e.g., Lin et al. 2006; Shou et al. 2011; Guo et al. 2016d; Zhang et al. 2017). However, debris-flow characteristics, formation mechanisms, and triggering conditions in different regions vary depending on the regional geological, geomorphological, and climatic conditions.

Coseismic landslides represent a major hazard type in the Lushan earthquake area, and many detailed investigations have been conducted on such phenomena with particular focus on their spatial distribution (Chen et al. 2014; Cui et al. 2014; Tang et al. 2015; Xu et al. 2015; Chang et al. 2016). For example, more than 1400 landslides and rockfalls have been described in the literature (Cui et al. 2014). It has been suggested that debris flows could be initiated from such identifiable landslides via increased pore water pressure at a slip surface (e.g., Iverson 1997, 2000; Montgomery et al. 2009; Baum et al., 2010), or by runoff through and erosion of loose material deposited in channels (e.g., Cannon et al. 2001; Gabet and Bookter 2008; Smith et al. 2012; Kean et al. 2013; Reid et al. 2016; Prenner et al. 2018, 2019; Simoni et al. 2020).

Following the event of the Lushan earthquake in 2013, debris flows have frequently occurred in the study region and many of considerable size occurred in dozens of gullies during August 20–22 2019. Such hazards have destroyed infrastructure (e.g., roads, houses, and hydropower stations), blocked rivers, and resulted in fatalities. However, the dominant formation process and the development mechanism of debris flows in the Lushan earthquake area have not been investigated fully. In addition, as a long-term consequence of earthquakes, the rainfall thresholds governing the triggering of debris flows are of importance for debris-flow forecasting, and their evolutionary tendency is of considerable scientific concern (Lin et al. 2008; Shieh et al. 2009; Huang et al. 2014; Guo et al. 2016a; Fan et al. 2018, 2019; Domènech et al. 2019; Li et al. 2018), both of which represent subjects that require comprehensive and systemic research.

In this study on debris flows in the Lushan earthquake area, we analyzed the spatial distribution and investigated their controlling factors and formation mechanisms.

Furthermore, we investigated the links between debris-flow occurrence and rainfall thresholds to reveal their spatial differences and elucidate their evolutionary tendency.

## 2 Study area

The study area is located in central Sichuan Province, southwestern China, and covers an area of ~4480 km<sup>2</sup>. It consists of two subbasins of the Baoxing River (BXR) and Lushan River (LSR; Fig. 1).

### 2.1 Geomorphology

The study area is located in a transitional region between the Sichuan Basin and the Tibetan Plateau; it is characterized by high mountains with elevations between 557 and 5291 m. The relief, which is higher in the northwest and lower in the southeast, is characterized by gorges with standing cliffs. The area has high coverage of vegetation (up to 60%) and the composition of the vegetation changes with altitude. Evergreen broadleaf forests occur at elevations below 1800 m, mixed evergreen and deciduous broadleaf forests occur between 1800 and 2300 m, mixed coniferous and broadleaf forests occur between 2300 and 2800 m, subalpine dark coniferous forests occur between 2800 and 3500 m, subalpine bush and meadow occur between 3500 and 4500 m, and alpine talus vegetation is found at elevations above 4500 m (Cui et al. 2014).

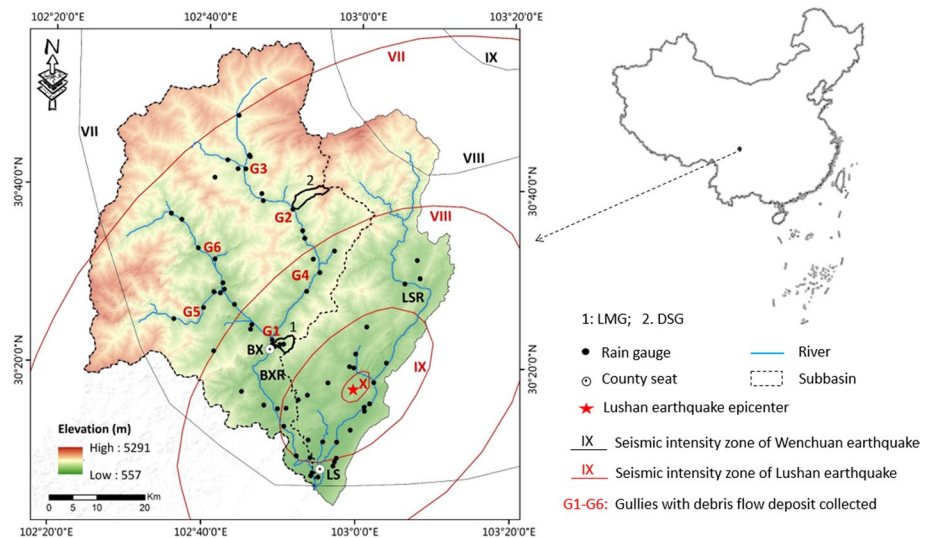


**Fig. 1** Topography and subbasins of the study area. Black circles denote rain gauge locations; red stars denote major earthquake epicenters

## 2.2 Faults and lithology

The Lushan earthquake (Fig. 1) occurred on the easternmost margin of the Tibetan Plateau, along a series of predominantly north–northeast-striking thrust faults that lie at the base of the Longmenshan Mountains on the northwestern edge of the Sichuan Basin. The main faults, which include the Jintang Arc Faults, Wulong Faults, and Longmenshan Faults, control the secondary faults and lithological development within the region. The Jintang Arc Faults comprise the Baoguoqiao and Qingpengshan faults as northern and southern branches. The Longmenshan Faults include the Shuangshi–Dachuan (S-DF) and Anxian–Guanxian faults (A-GF) (Fig. 2). Of these, it has been proposed that the S-DF was the seismogenic fault responsible for the 2013 Lushan earthquake (Zhang et al. 2013; Chen et al. 2014).

The lithology of the LSR is dominated by shale, siltstone, and sandstone. In the BXR, the lithology comprises volcanic (granite, diorite, and basalt), carbonate (limestone and dolomite, with some mixed or interlayered sand and mudstone that is generally easily deformed), and soft metamorphic (slate and phyllite) series. Loose Quaternary sediments

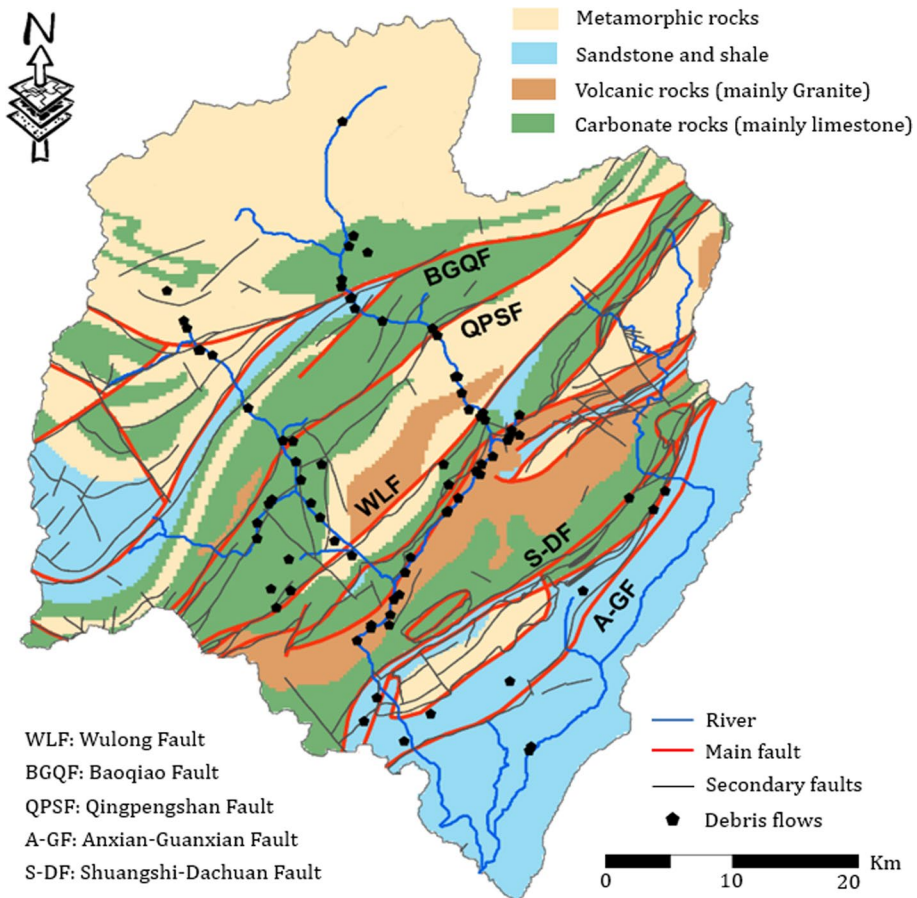


Fig. 2 Simplified geological map and historical debris-flow sites of the study area

(fluvial sand and gravel deposits) are occasionally found in the form of terraces and alluvial fans.

## 2.3 Climate

The study area is situated in a subtropical and humid monsoon climatic zone. Annual average rainfall in Baoxing (BX) and Lushan (LS) counties is 1313 and 1101 mm, respectively. More than 70% of the rainfall occurs in the rainy season (June–September). Generally, short-duration rainstorms and high-intensity rainfall are important factors in relation to debris-flow hazards (Guo et al. 2016a). The spatial distributions of 24- and 1-h maximum rainfall are shown in Fig. 3a and b, respectively. It can be seen that rainfall increases from the northwest to the southeast. According to data recorded at the LS and BX meteorological stations, which have both been located in their respective county seats since the 1950s, the multiyear average maximum 24-h rainfall in LS and BX counties is 108 and 58 mm, respectively, while the historical maximum value is 188 and 123 mm. The multiyear average maximum 1-h rainfall in LS and BX counties is 50 and 45 mm respectively, while the historical maximum value is 86 and 68 mm, respectively (Fig. 3).

## 3 Data source and methods

The debris-flow data, which included not only the historical occurrence time, spatial location, and volume of each debris-flow event, but also the sediment deposit conditions associated with the time of construction and position of debris-flow control works, were provided by the local Land and Resources Department. Overall, 54 debris-flow sites with occurrence history were recorded. As field surveys were periodically performed after the rainy season, and detailed investigations were undertaken following the occurrence of each significant hazard event, the data were considered complete and reliable.

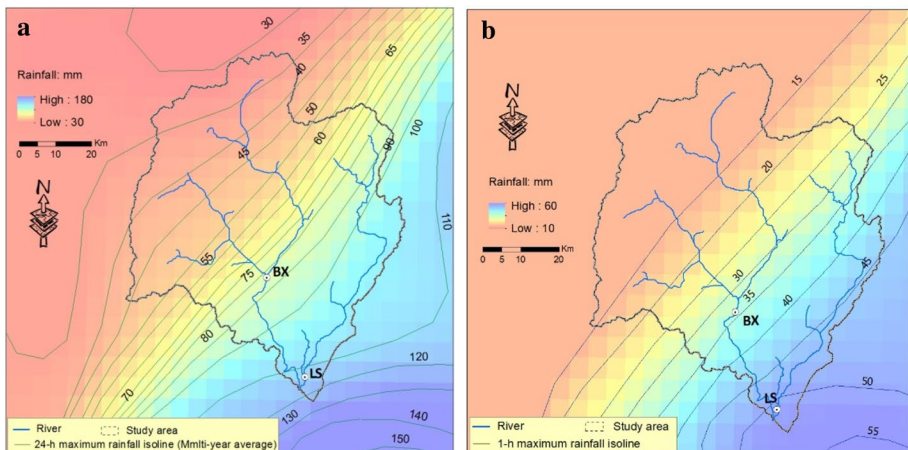


**Fig. 3** Spatial distribution of historical maximum rainfalls: **a** 24-h rainfall and **b** 1-h rainfall

Specific field investigations using common measuring devices were also performed after each debris-flow event to help establish the formation process. For example, range finders were used to measure the flow height ( $h$ ) and channel section width ( $L$ ). Using traditional velocity calculation methods (Costa 1984; Richenmann 1999), flow velocity ( $v$ ) was estimated based on the slope gradient ( $I$ ) measured in the field, the flow height ( $h$ ), which was estimated based on field evidence, and an empirical constant ( $C$ ), which is generally determined from a lookup table. Remote sensing imagery obtained by an unmanned aerial vehicle was also employed together with field-based approaches to evaluate the spatial distribution of the solid material. The equations used to calculate the flow velocities and discharges can be expressed as follows:

$$v = CH^a I^b \quad (1)$$

$$Q = vA \quad (2)$$

where  $v$  is the flow velocity (m/s),  $C$  is an empirical constant,  $H$  is the flow depth (m),  $I$  is the channel bed gradient,  $Q$  is the flow discharge (m<sup>3</sup>/s), and  $A$  is the cross-sectional area (m<sup>2</sup>), which was taken as the product of the flow height and channel width.

When calculating water flow velocity, the values of  $a$  and  $b$  are set as 2/3 and 1/2, respectively, and Eq. 1 is equivalent to the Manning equation, where  $C$  can be represented by the Manning coefficient  $n$ , the recommended value of which for a neighboring mountainous watershed in southwestern China is 0.08 (Cui et al. 2018). When using Eq. 1 for calculation of a viscous debris flow, it is recommended that the values of  $a$  and  $b$  be set as 0.3 and 0.5, respectively, and Eq. 1 turns into the Chezy equation, for which the recommended value of  $C$  is approximate 10 (Richenmann, 1990; Koch 1998).

The rainfall data used in this study were provided by national and local meteorological departments. The rain gauge network in this region is dense and covers the region of debris-flow occurrence (Fig. 1). For most debris-flow sites, rainfall measurements from nearby rain gauges allow high-precision analysis. In this study, data from 67 gauges were used and the hydrological data were provided by the local hydrographic bureau.

The rainfall thresholds for triggering debris flows were analyzed following a previously proposed method based on the relationship between rainfall intensity and rainfall duration (Caine, 1980; Jibson 1989; Aleotti 2004; Gabet et al. 2004; Cannon et al. 2008; Guzzetti et al. 2007, 2008; Saito et al. 2010; Guo et al. 2013, Guo et al. 2016b; Berti et al. 2020). The threshold curve was assumed to take the form of a power law:

$$I = aD^{-b} \quad (3)$$

where  $a$  and  $b$  are constants,  $D$  is rainfall duration (h), and  $I$  is mean rainfall intensity in the period of  $D$  (mm/h).

## 4 Results

### 4.1 Spatial distribution of debris flows

#### 4.1.1 Historical debris flows before 2018

Debris flows were rarely reported before the 2008 Wenchuan earthquake, and according to local land department records and field interviews, they only occurred infrequently in



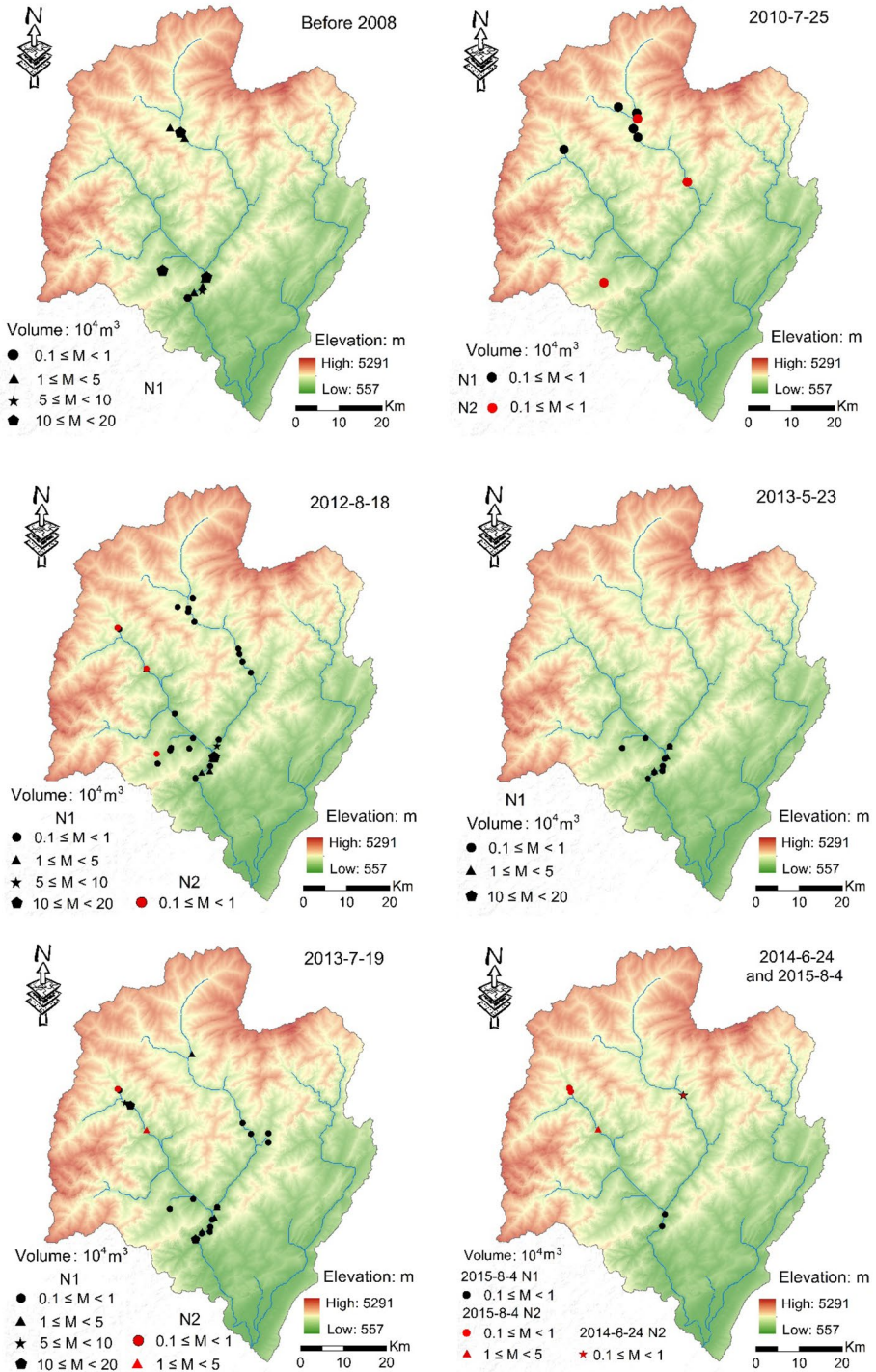


Fig. 4 Distribution and volume of historical debris flows

certain tributaries. However, after the Wenchuan earthquake, debris flows began to occur more frequently following rainstorms (Fig. 4). These flows were not only formed by natural landslides and/or channel material failures, but also by engineering residue (e.g., hydro projects, road construction, and mining). Deposit volumes generally vary in the range of  $0.1\text{--}40 \times 10^4 \text{ m}^3$ . In this study, based on deposit volume, debris flows were classified into five intervals:  $0.1\text{--}1 \times 10^4$ ,  $1\text{--}5 \times 10^4$ ,  $5\text{--}10 \times 10^4$ ,  $10\text{--}20 \times 10^4$ , and  $> 20 \times 10^4 \text{ m}^3$ . In addition, based on material supply, debris flows were further classified into two types: N1 and N2. The former group included debris flows supplied from natural slopes and/or channel materials, while the latter group comprised debris flows formed from engineering waste deposits.

In 2010 and 2012, after the 2008 Wenchuan Earthquake, debris-flow numbers increased (Fig. 4b and 4c). The debris-flow events of August 18 2012 were of particular concern because one of the sites (LMG in Fig. 1) was close to BX County. The volume of the event was approximately  $10 \times 10^4 \text{ m}^3$  and the debris flow caused considerable damage, including

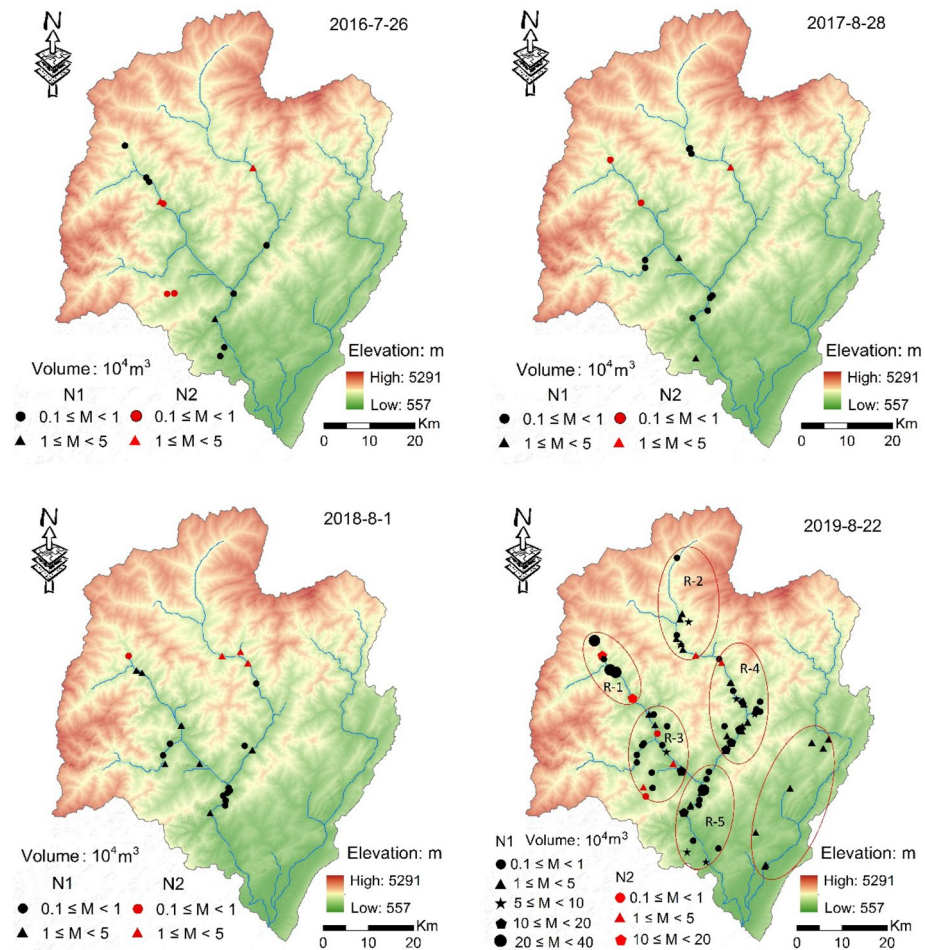


Fig. 4 (continued)



the destruction of houses and roads and blockage of the river (Wang and Xie, 2016). High-intensity and short-duration rainstorms were the main triggering factor for this debris flow. In the 6 h before the flow occurred, the accumulated rainfall amount was 97 mm and the maximum 1-h rainfall intensity was 55.9 mm/h.

The 2013 Lushan earthquake inevitably stimulated further debris-flow activity. Shortly after the earthquake's occurrence, debris flows were triggered twice in more than 20 gullies during the rainy season. The May 23 2013 event was concentrated primarily in the middle section of the BXR. The triggering rainfall had short duration (<3 h). The accumulated total and peak intensity of the rainfall measured at various rain gauges were 28.6–47.7 mm and 22.1–31.4 mm/h, respectively. During the July 9 2013 event, the spatial scope of the debris flows expanded further to include the entire BXR basin. According to historical records, some gullies experienced their first ever debris flows during this event. The rainfall amounts responsible for this event were in the range of 54.7–63.5 mm, and the peak rainfall intensities were 8.2–8.9 mm/h. Both the triggering rainfall amounts and the peak rainfall intensities were much lower than those of the 2012 event; nevertheless, the newly developed gully debris flows had much greater volumes. The reason was the increased quantity of available loose material, which was attributable to the 2013 Lushan earthquake. This supply of loose material could feed debris flows, even following the relatively lower amount of rainfall. During 2014–2018, debris flows occurred frequently and widely throughout the region. However, the volumes were relatively small, i.e., none was greater than  $10 \times 10^4 \text{ m}^3$ .

#### 4.1.2 Debris flows in 2019

The debris flows that followed the rainfall event of August 19–22 2019 are regarded as the most disastrous in the historical record. The duration of the rainfall recorded at most rain gauges was from 00:00 (LT) on August 19 to 20:00 on August 23. The rainfall amount measured at most gauges was in the range of 150–300 mm, with minimum, average, and maximum values of 110.2, 240.3, and 494.0 mm, respectively. The peak intensity at most gauges was in the range of 20–30 mm/h, with minimum, average, and maximum values of 11.3, 25.3, and 51.0 mm/h, respectively. The spatial distributions of peak rainfall intensity and total rainfall amount of this event, interpolated from the rain gauge data, are shown in Fig. 5.

The runoff observed at several hydrometric stations along the main rivers provided a reference for the climatic and hydrological conditions pertaining during this event. The water discharge observed at Wulong Station (Fig. 5) was  $650 \text{ m}^3/\text{s}$  at 12:00 on August 22, and the return period was over 40 years. The water discharge at Baoxing Station was  $1650 \text{ m}^3/\text{s}$  at 12:10 on August 22, and the return period was over 100 years. The water discharge at Lushan Station was  $4900 \text{ m}^3/\text{s}$  at 12:00 on August 22, and the return period was also over 100 years. The event is regarded as the maximum observed flood since the establishment of all three stations. During this event, debris-flow activity was not limited to only one or a few gullies; instead, it was recorded in almost all systems concurrently. The debris flows mainly occurred along the BXR with activity recorded in 44 gullies. Among them, 23 were identified as new (i.e., it was the first time a debris flow had occurred in that gully). In the LSR, six gullies were recorded as having debris flows and all were new.

The volumes of the debris flows were higher than those of historical events. Debris flows in 10 gullies had a volume of  $> 10 \times 10^4 \text{ m}^3$ , of which 4 were  $> 20 \times 10^4 \text{ m}^3$  (maximum volume:  $39.6 \times 10^4 \text{ m}^3$ ). Many flows were supplied by engineering waste material

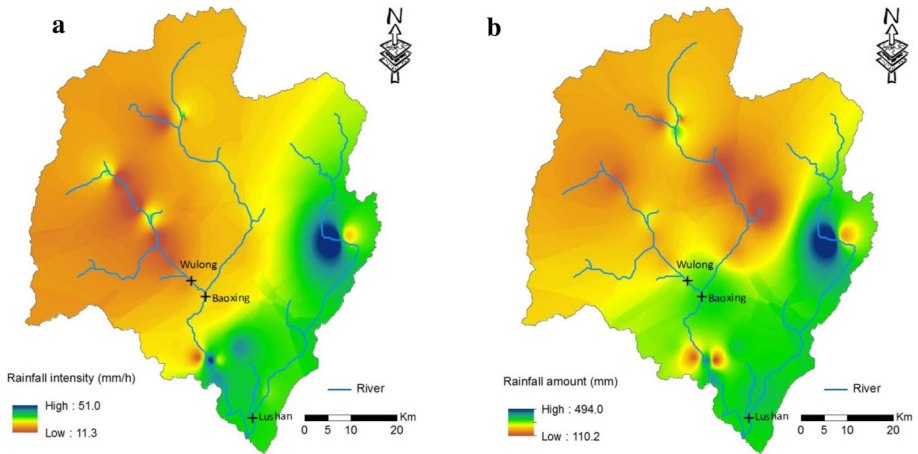


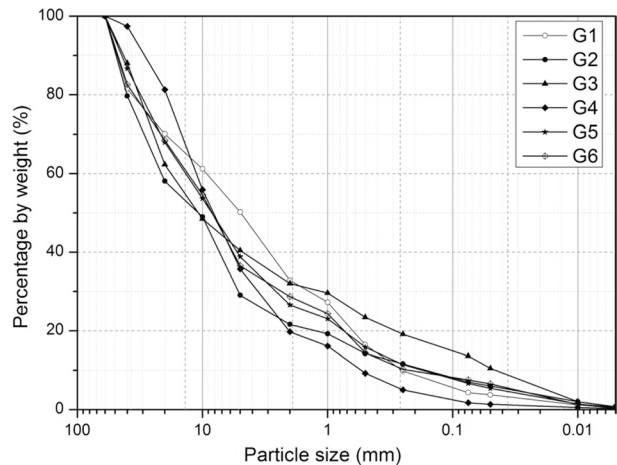
**Fig. 5** Spatial distribution of rainfall in the August 22 2019 event: **a** peak intensity and **b** rainfall amount

(Fig. 4j). According to field investigation and sample analysis, the flows were generally viscous. We collected samples (particle size: < 10 mm) of the deposits in the fans of the gullies indicated in Fig. 1. The proportion of fine particles (diameter: < 0.075 mm) was in the range of 3.8–26.78%, with a mean value of 14.23% (Fig. 6), i.e., higher than found in the debris flows in the Wenchuan earthquake area (Cui et al. 2018).

#### 4.1.3 Debris-flow spatial distribution

Debris flows in the study area likely occurred in all lithological regions, similar to those in the Wenchuan earthquake area, suggesting the indiscriminate influence of earthquakes on debris flows (Guo et al. 2016b). Overall, fault activity is the controlling factor of debris-flow formation. Comparatively, debris flows occurred more extensively and frequently in the BXR basin, within which secondary faults are distributed more densely than in the

**Fig. 6** Grain size composition of debris-flow deposits with particles < 10 mm (G1–G6 denote samples collected in different gullies, see Fig. 1)



LSR basin (Fig. 2). Most of the faults trend in the NE–SW direction, as do the main faults, and they cross the small watersheds. The dense distribution of faults and the frequent seismic activity have resulted in widespread breakage of rocks.

The middle section of the BXR hosts the southern branch of the Wulong Fault, which marks the boundary between carbonate and volcanic rocks and controls the direction of the eastern branch of the BXR. Owing to the dense faulting and the frequent seismic activity, cleavages and fissures have developed in the hard volcanic rock (Fig. 2). The carbonate rocks are mixed with sand and mudstone and are sometimes interlayered with muddy bands that tend to soften and deform under weathering action. This destroys the integrity of the carbonate rock masses and allows enhanced weathering, which creates the loose material.

Another area prone to debris-flow activity is the upper stream of the west branch of the BXR, which is dominated by highly weathered soft metamorphic rocks. Slate and phyllite, which are generally formed by regional dynamic metamorphism, are weak and contain cleavage fissures.

In addition to the geological and topographic conditions, the distribution of debris-flow locations in each rainstorm event is mainly dominated by the local rainfall distribution. For instance, during the May 23 2013 event, local rainfall was concentrated in the middle section of the BXR, as was the debris-flow distribution. During the August 22 2019 event, although debris flows occurred widely throughout the basin, centers of heavy rainfall in southern and eastern parts of the study area produced debris flows with greater magnitude. In particular, the heavy rain in the LSR basin (Fig. 5) caused new debris flows.

## 4.2 Debris-flow formation processes and mechanisms

Here, typical debris-flow events in two gullies are introduced and used to identify the formation processes and mechanisms.

### 4.2.1 LMG debris flow on August 18 2012

Lengmu gully (LMG) covers an area of 9.44 km<sup>2</sup> and is located along the middle section of the BXR (Fig. 1). The channel length is 5.63 km, and the gradient is 212%. The highest elevation is 3044 m on the ridge and the lowest elevation is 996 m at the gully mouth. It has a ‘horn’ shape and it consists of six subsidiary branches. Vegetation coverage is over 70% (Fig. 7). A debris flow in this watershed first occurred following the rainfall event of August 18 2012.

The precipitation event responsible for this debris flow, which produced a total rainfall amount of 98 mm and a peak intensity of 56.8 mm/h, was concentrated during the period of 02:00–03:00 (Fig. 7a), with antecedent rainfall of 5.7 mm on the day before. This short-duration and high-intensity rainfall is a typical example of an event that can easily stimulate flash floods in small catchments.

The debris-flow soil sources consisted of loose material accumulated in channels and landslides, and shallow unstable slopes along the channels. Field investigation after the debris-flow event identified 10 fragile sections (Fig. 7b) with erodible bed compositions and a total volume of approximately  $111 \times 10^4$  m<sup>3</sup>. It was estimated that this material contributed  $19.4 \times 10^4$  m<sup>3</sup> of material to the debris flow, whereas shallow slope failures contributed only  $0.8 \times 10^4$  m<sup>3</sup> of material to the debris flow.

The watershed was divided into three regions: I, the headwater region; II, the debris-flow formation and development region; and III, the debris-flow deposition region

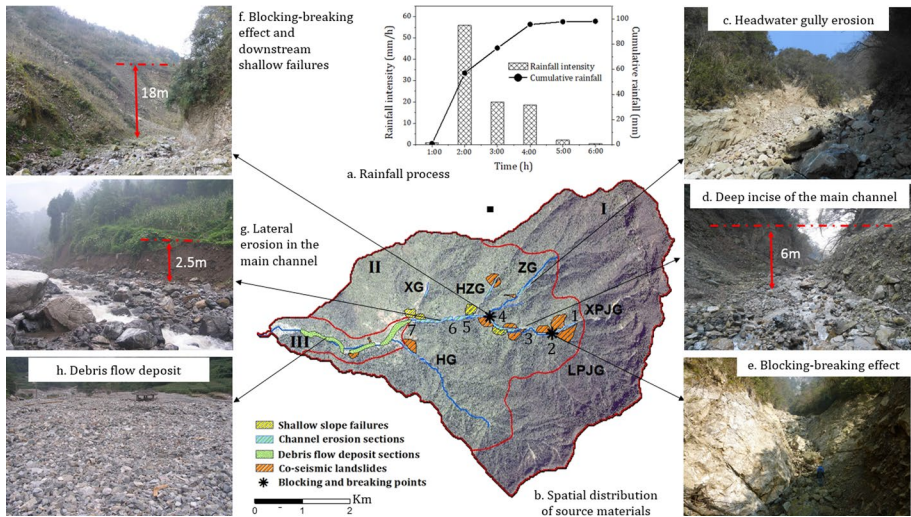


Fig. 7 Source material distribution and debris-flow development process

(Fig. 7b). In region I, the bedrock is almost complete. There is high coverage of vegetation and very little sediment in the channels. The water runoff yield likely accumulated quickly in this region. Using Eq. 1, the flow discharge was calculated to be  $49.9 \text{ m}^3/\text{s}$  in Sect. 1 (Fig. 8). The debris-flow source material was mainly distributed in region II across the elevation range of 1300–1900 m, and along a total channel length of approximately 1.8 km. Naturally unstable slopes, downhill colluvial deposits, and Quaternary sediments from old debris-flow deposits are widely distributed along the channel. Here, channel erosion caused by intense water runoff in headwater regions is evident and significant in all tributaries (Fig. 7c). The flow was also amplified by deep incision along the channels (Fig. 7d). For

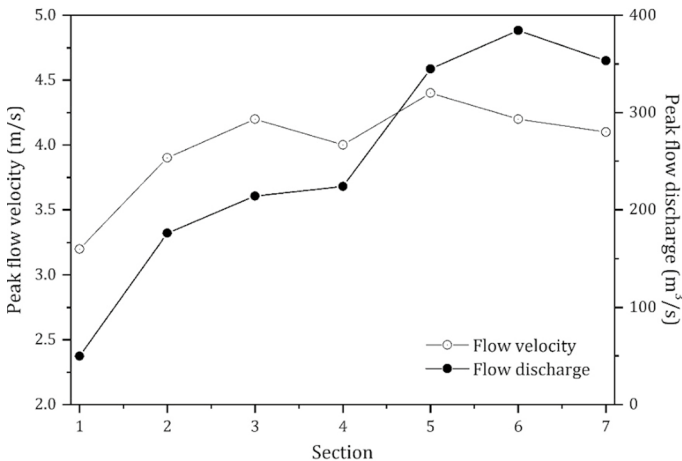


Fig. 8 Peak velocity and peak discharge of debris flow along the channel

example, in the LPJG tributary (Sects. 1–2 in Fig. 7b), the channel was incised by an average depth of approximately 3–4 m, with a maximum value of 8.0 m in a 500-m straight steep ( $\approx 13^\circ$ ) channel. The peak velocity and discharge at the end of this channel section were calculated as 3.9 m/s and 176.0 m<sup>3</sup>/s, respectively. In Sects. 3–4, the channel was incised by approximately 4–5 m, with a maximum value of 10.0 m in a 700-m straight steep ( $\approx 10^\circ$ ) erodible channel. The peak discharge and velocity of the flow were amplified substantially to 224.2 m<sup>3</sup>/s and 4.2 m/s, respectively. Narrow and constrictive sections with bedrock on one side and soil slopes on the other were also identified in the channel (Fig. 7e and f). At these points, debris flows could accumulate, with areas upstream becoming blocked, following which outbursts could occur through failure of the soil on the weaker side. The peak discharge measured for Sect. 4 was up to 344.8 m<sup>3</sup>/s.

After Sect. 4, although lateral erosion of the loose diluvium slope occurred along the channel, channel incision remained the main contributor to debris-flow development. Here, the channel slope varies but it is always steep, with an average gradient of 165‰. The average incision depth is 1–2 m, with a maximum value of 2.5 m (Fig. 7g). The flow peak discharge varied but ultimately reached 353.4 m<sup>3</sup>/s. The variations of the peak flow velocity and peak flow discharge of the debris flow along the channel are illustrated in Fig. 8.

The debris flows deposited material with a total volume of approximately  $10.14 \times 10^4$  m<sup>3</sup> in the downstream area of the watershed. However, approximately  $10 \times 10^4$  m<sup>3</sup> of material outflowed the watershed and blocked the river and was ultimately washed and/or swept away (Wang and Xie 2018). The deposited material comprised boulders with diameters of 1–2 m, which accounted for 10%–15% of the total volume, gravel (diameter: 20–100 cm), which accounted for 50–60% of the total volume, gravel (diameter: < 20 cm) and sand, which accounted for 30–40% of the total volume, and clay; such material is typical of viscous debris flows.

It should be noted that the volume of available source material increased substantially after the 2013 Lushan earthquake, with  $> 123 \times 10^4$  m<sup>3</sup> of material within 17 new coseismic landslides and/or shallow failures (Fig. 7b). This volume of material has high potential to fail following rainstorms and will supply future debris flows.

#### 4.2.2 DSG debris flow on August 22 2019

Desheng gully (DSG) is located in the upstream section of the BXR (Fig. 1). The watershed area is 2.86 km<sup>2</sup>, and the gully length is approximately 3.5 km. The highest and lowest elevations are 3493 and 1745 m, respectively, and the overall channel gradient is 264%. The vegetation coverage is  $> 75\%$  (Fig. 9a) and debris flows were not recorded before 2019.

Rainfall continued for 53 h after starting at 19:00 on August 20 2019. Antecedent rainfall on August 18 and 19 totaled 24.6 mm. The total accumulated rainfall of this event was 100.8 mm, with peak intensity of 23.8 mm/h at 05:00 on August 22; according to local residents, this coincided with the debris-flow occurrence time (Fig. 9b).

The potential solid material on the slopes and in the channels is shown in Fig. 9a. Bare bedrock can be observed in the images, and these areas were identified as shallow slopes and/or landslides in the headwater regions (Region HW in Fig. 9a). The total potential material volume is  $3.5 \times 10^4$  m<sup>3</sup>; however, this material was not the main contributor to this debris flow. Field investigation revealed that at Sect. 1 (S1), the flow was better categorized as a waterflood; we observed no evidence of solid material deposits but did identify flood washing traces. The flow cross-sectional area was identified based on flood marks (e.g., shrubs and grass aligned in the same direction along a



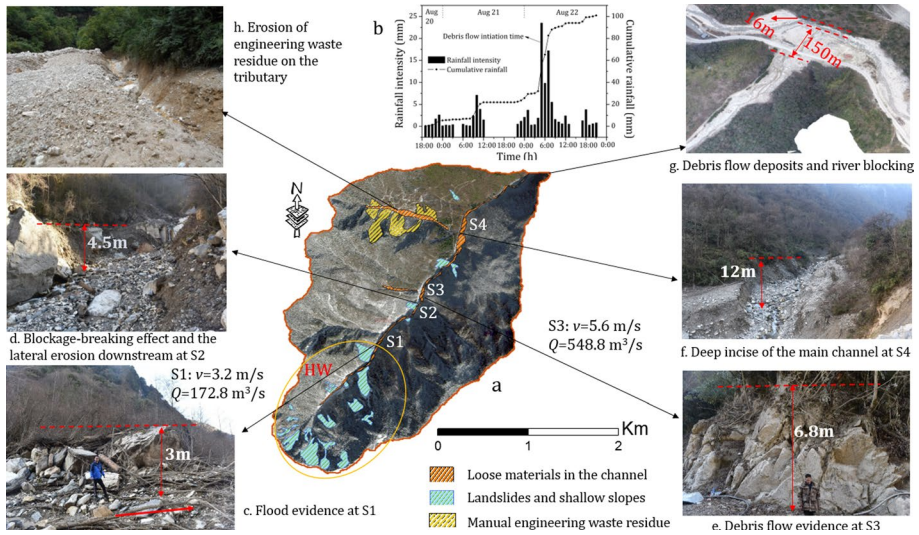


**Fig. 9** Spatial distribution of material sources and debris-flow formation processes in Desheng gully (DSG)

near-horizontal line; Fig. 9c). The flow velocity and discharge in this area were calculated as 3.2 m/s and  $172.8 \text{ m}^3/\text{s}$ , respectively.

Downstream of S1, the debris flows were initiated by lateral erosion and deep incision of the channel. The channel bed is comprised of Quaternary sediments, including ancient slope and debris-flow deposits covered by vegetation. However, these deposits were eroded substantially by surface runoff during the rainfall event. Along section S1–S2, the average incision depth is 3–4 m, with a maximum depth of 6.0 m. It is apparent that blockages occurred in areas where the channel narrowed between the bedrock on one side and the erodible soil slope on the other. Such blockages increased the discharge, and also caused further lateral erosion and/or incision downstream (Fig. 9d). For instance, at S3, located approximately 150 m downstream of the S1 blockage point, debris-flow marks are evident and mud is found horizontally on one side of the channel (Fig. 9e). According to a local witness, “The flow was turbid and turbulent, consisting of water, rocks, boulders, and mud. The flow moved very rapidly and rose to a height greater than that of a house.” The peak velocity and discharge were estimated as 5.6 m/s and  $548.8 \text{ m}^3/\text{s}$ , respectively.

Downstream of S3, the channel is straight for 1.2 km; here, the channel is erodible and there is a thick (> 10 m) layer of Quaternary sediments on both sides. In this area, deep incision and lateral erosion are more substantial. The average erosion depth is 5–6 m with a maximum depth of up to 12 m. This region contributed a considerable volume of material (Fig. 9f); ultimately, the debris flows destroyed four houses, buried the road and blocked the river with approximately  $20 \times 10^4 \text{ m}^3$  of material (Fig. 9g).

In addition to natural material, engineering residue is abundant in the left-hand tributary of the DSG (Fig. 9a). This material includes a greater clay content and fewer boulders, which in general makes it very prone to debris flows (Fig. 9h). Even on a normal day, the flow in this tributary is muddy. During the August 22 event, the debris flow had a huge volume ( $4.5 \times 10^4 \text{ m}^3$ ) and deposited a substantial amount of material in the main channel.

### 4.2.3 Debris-flow formation mechanisms

The solid material sources for debris flows include: (1) slope failures (landslides and shallow failures), (2) loose material in and/or along channels, and (3) other artificial loose material in the watershed (e.g., waste material from mining, hydro projects, and road construction).

Although earthquakes can cause slope instabilities and landslides/shallow failures exist naturally, they are not considered the main drivers of debris-flow formation and they generally contribute only a small proportion to the total volume. Instead, the abundant loose materials in the original channel, which generally consists of and/or accompanies erodible Quaternary sediments (e.g., slope sediments and old debris-flow deposits), are the main source for debris flows.

Loose material can be eroded rapidly and substantially by high-velocity runoff (Fig. 10a and b). The surface flow in steep headwater channels concentrates loose material, which then contributes to erosion of further material along the bed, similar to the ‘progressive bulking’ effect (Griffiths et al. 2004; Godt and Coe 2007; Imaizumi et al. 2006, 2019; Coe et al. 2008; Gregoretto and Fontana 2008; McGuire et al. 2017; Ma et al. 2018; Berti et al. 2020). The process of channel incision exposes a free surface of diluvium along the channel, which can experience subsequent and severe lateral erosion (Fig. 10c). The channel bed was composed of either coarse loose material from slope failures at local lower-gradient sections or fine weakly consolidated soils, which are highly prone to runoff erosion. This phenomenon is very common in this region (Fig. 10d), and the process of successive incision and erosion of channels is regarded as the primary driver of sediment entrainment, playing a key role in the transformation of a water flow into a debris flow.

As mentioned above, narrow channel sections, usually with bedrock on one side and a loose slope on the other, are also common in the watersheds. There is potential for debris flows to become blocked in such narrow sections; however, when en masse failure of the loose slope is caused by outburst of the blockage, the debris-flow volume and velocity can be amplified substantially. This breaking effect of the cross section has also been reported

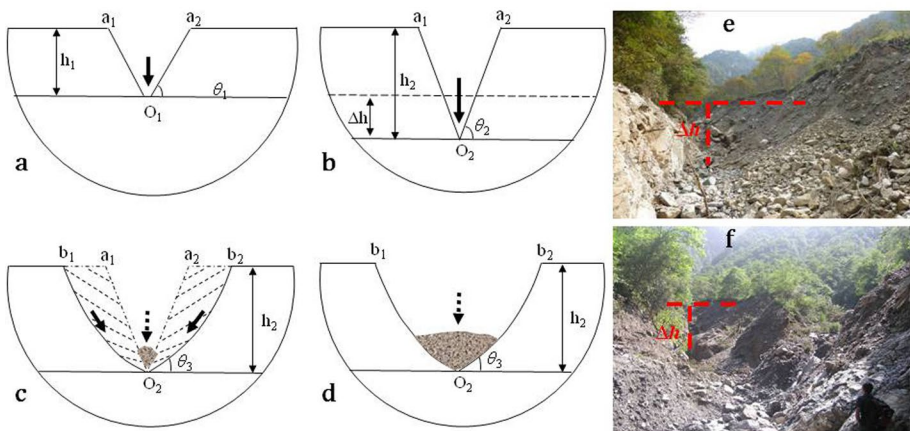


**Fig. 10** Debris-flow formation process.  $O_1$ : initial channel elevation,  $O_2$ : ultimate channel elevation,  $a_1$  and  $a_2$ : the original channel width,  $b_1$  and  $b_2$ : ultimate channel width,  $h_1$  and  $h_2$ : original and ultimate erodible channel height,  $\Delta h$ : height of erosion, and  $\theta_1$ - $\theta_3$ : slope gradient

in other regions (Bardou and Jaboyedoff 2008; Cui et al. 2013; Kean et al. 2013; Tang et al. 2020).

### 4.3 Rainfall thresholds

#### 4.3.1 Rainfall conditions responsible for debris flows

Generally, debris flows are more likely to be triggered by intense rainfall over a short period. Most of the debris flows of the August 18 2012 event were triggered by rainfall with intensity of 28.6–47.7 mm over a 3-h period. In the August 22 2019 event, although the duration of the rainfall was long, the debris flows occurred during the period of peak intensity (mean intensity: 25.3 mm/h). As intense rainfall generally causes rapid flash floods in mountainous catchments, this highlights the prominent effect of surface channel runoff in debris-flow formation.

Given the importance of rainfall to debris-flow occurrence, we analyzed the rainfall conditions of the events from the perspective of the  $I_T$ - $R$  relation and the commonly used intensity–duration ( $I$ - $D$ ) method (e.g., Caine 1980; Chen et al. 2005; Guzzetti et al. 2007, 2008; Cannon et al. 2008; Guo et al. 2016a, b; Berti et al. 2020). Among the rainfall parameters,  $I_T$  represents the triggering rainfall intensity (mm/h) at the time of debris-flow occurrence,  $R$  (mm) is the cumulative amount of rainfall in the period from the start of the rain event to the time of debris-flow occurrence ( $D$ , unit: h), and  $I$  is the mean rainfall intensity (mm/h) in period  $D$ .

Overall, debris flows can be divided into two classes according to their source. Normal debris flows are supplied by natural solid materials in and/or along the channel. They require higher rainfall conditions, i.e., average values of  $R$  and  $I_T$  of 48.8 mm and 20.0 mm/h, respectively. Other debris flows that are initiated by engineering waste mixing with runoff require lower rainfall conditions, i.e., average values of  $R$  and  $I_T$  of 19.7 mm and 8.2 mm/h, respectively.

The rainfall  $I$ - $D$  threshold is determined as follows:

$$I = 8.38D^{-0.65} (1 \text{ h} \leq D \leq 29 \text{ h}) \text{ for debris flows supplied by natural sources.} \quad (4)$$

$$I = 4.16D^{-0.45} (2 \text{ h} \leq D \leq 14 \text{ h}) \text{ for debris flows supplied by engineering waste material.} \quad (5)$$

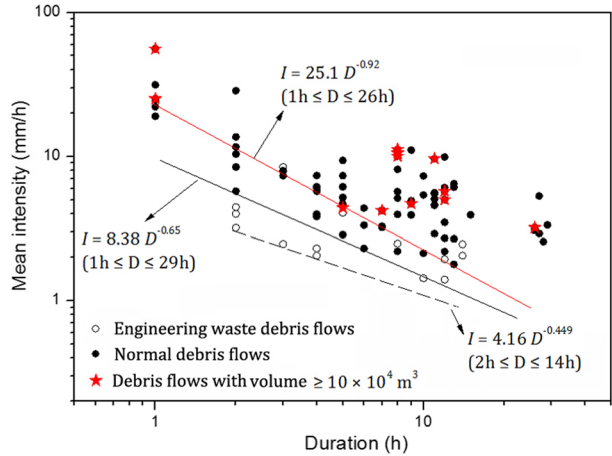
#### 4.3.2 Rainfall thresholds for high-volume debris flows

Most debris flows in the study region have volumes of  $< 5 \times 10^4 \text{ m}^3$ . However, in certain events with extensive rainfall, grouped debris flows were observed and debris flows with larger volumes ( $> 10 \times 10^4 \text{ m}^3$ ) caused substantial damage (e.g., the July 9 2013 and August 22 2019 events). In this work, we defined thresholds for these high-volume debris flows by analyzing the  $I$ - $D$  relationship (Fig. 11):

$$I = 25.1D^{-0.92} (1 \text{ h} \leq D \leq 26 \text{ h}) \quad (6)$$

which is much higher than that for normal debris flows, as expressed in Eqs. 4 and 5.

**Fig. 11** Rainfall intensity–duration (*I*-*D*) thresholds for debris flows



### 4.3.3 Spatial differences in rainfall conditions required for debris flows

The study region covers an extensive area, over which rainfall varies with elevation. Rainfall isolines (Fig. 3) show that rainfall is lower in the northwest and higher in the southeast, resulting in differences among the upper, middle, and lower sections of the rivers. Furthermore, the topographic and geological conditions also differ. We divided the study area into six subregions according to debris-flow distribution (Fig. 4), elevation, and the main exposed lithologies:

- R-1: upper stream of the west branch of the BXR; elevation range of 2500–2000 m and predominantly slate and phyllite lithologies;
- R-2: upper stream of the east branch of the BXR; elevation range of 2600–2100 m and predominantly limestone lithology;
- R-3: downstream of the west branch of the BXR; elevation range of 1200–1700 m and predominantly limestone lithology;
- R-4: downstream of the east branch of the BXR; elevation range of 1200–1900 m and predominantly limestones and granites cut by the Wulong Fault;
- R-5: mainstream of the BXR, downstream of the confluence of the west and east branches; elevation range of 750–1200 m and predominantly granite lithology;
- R-6: main stream of the LSR; elevation range of 750–1400 m and predominantly sandstone lithology.

The triggering rainfall intensities and inducing rainfalls are shown in Fig. 12. Debris flows in R-3 and R-4, the downstream branches of the BXR, require the lowest rainfall amount (amount: 13.8 and 14 mm, intensity: 7.5 and 5.5 mm/h, respectively). R-1, the headwater of the western branch and R-5, the mainstream of the BXR, require similar rainfall intensities to trigger debris flows (8.1 and 8.8 mm/h, respectively); however, the inducing rainfall in R-1 (19.0 mm) is higher than in R-5 (16.3 mm). Debris flows in R-2 require the highest rainfall conditions (amount: 23.2 mm, intensity: 12.0 mm/h). Overall, the rainfall conditions needed for debris flows in LSR are much higher than in BXR.

The proposed *I*-*D* thresholds are shown in Fig. 13. It can be seen that R-3 and R-4 are most prone to debris flows, and that the rainfall threshold in R-6 is much higher than

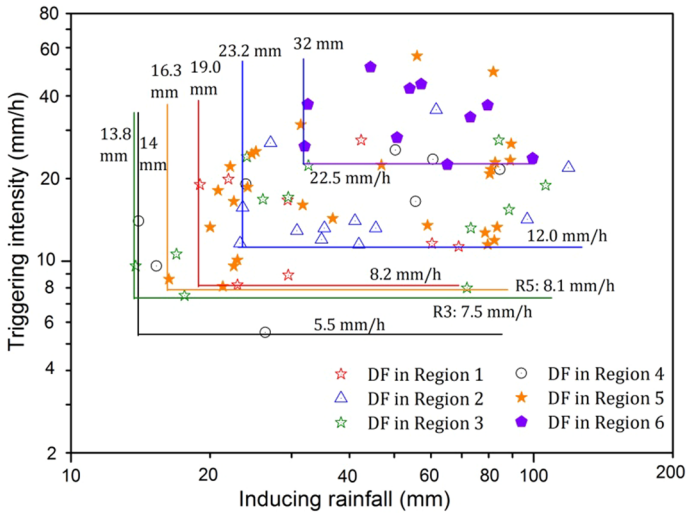


Fig. 12 Inducing rainfall and triggering rainfall intensity in the subregions

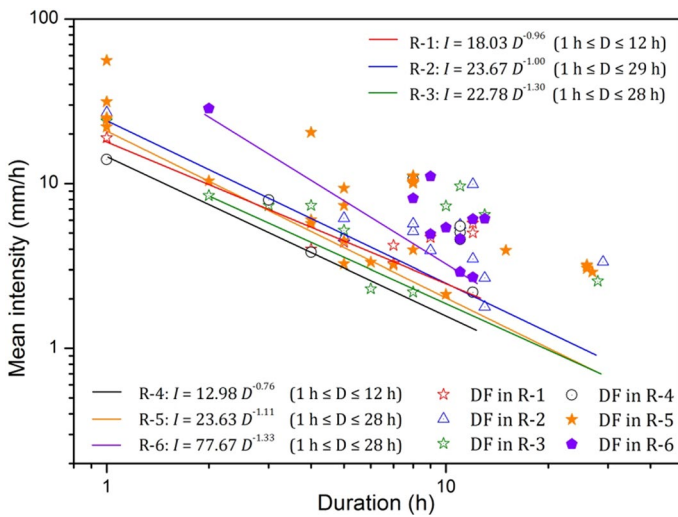


Fig. 13 Rainfall thresholds for debris-flow occurrence in the subregions

other regions. This indicates that debris flows occur most easily in the elevation range of 1200–1700 m and where the main lithology is limestone. This also highlights the controlling effect of the seismic activities of the dense faults on debris-flow occurrence in R3 and R4 (Fig. 2).

#### 4.3.4 Temporal variations in rainfall conditions required for debris flows

Temporal variations in the rainfall thresholds for debris-flow occurrence were investigated by dividing the study period into three intervals: (1) 2010–2012: after the 2008 Wenchuan



earthquake and before the 2013 Lushan earthquake; (2) 2013–2017: shortly after the Lushan earthquake, with the five-year time span selected based on research into the Wenchuan earthquake area (Guo et al. 2016c; Cui et al. 2018); and (3) 2018–2019: more than five years after the Lushan earthquake.

Rainfall thresholds were estimated as expressed in Eq. 6 and are illustrated in Fig. 14. The rainfall thresholds for debris flows after 2013 were much lower than for those that occurred before 2013, indicating that the earthquake event reduced the thresholds. The thresholds in 2018 and 2019, i.e., more than five years after the earthquake, were higher and similar to those before the earthquake. This likely reflects the effect of both the humid climate and the high rate of vegetation recovery, but also the reduction in the availability of solid material over time; however, this is not to say that the debris flows were stable. Although the threshold rainfall conditions recovered, debris flows were distributed more widely and had much greater volumes.

$$\begin{aligned}
 a. I &= 17.15D^{-0.85} (1 h \leq D \leq 6 h) \\
 b. I &= 7.63D^{-0.58} (1 h \leq D \leq 29 h) \\
 c. I &= 27.34D^{-1.13} (2 h \leq D \leq 12 h)
 \end{aligned}
 \tag{7}$$

### 5 Discussion

Although the 2013 Lushan earthquake inevitably decreased slope stability, the coseismic landslides were not the main source of solid material driving debris flows that occurred in the following the years. On the contrary, results suggested that the erosion of channel deposits by overland runoff was the dominant mechanism of debris-flow formation. It is generally difficult to identify the initiation location of runoff-generated debris flows owing

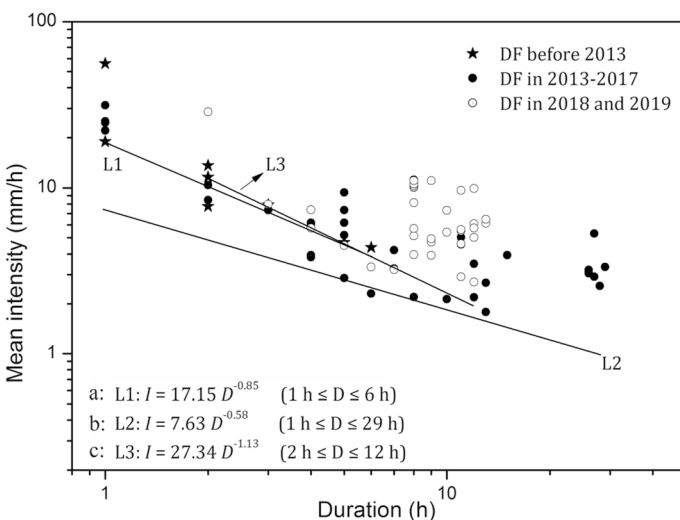
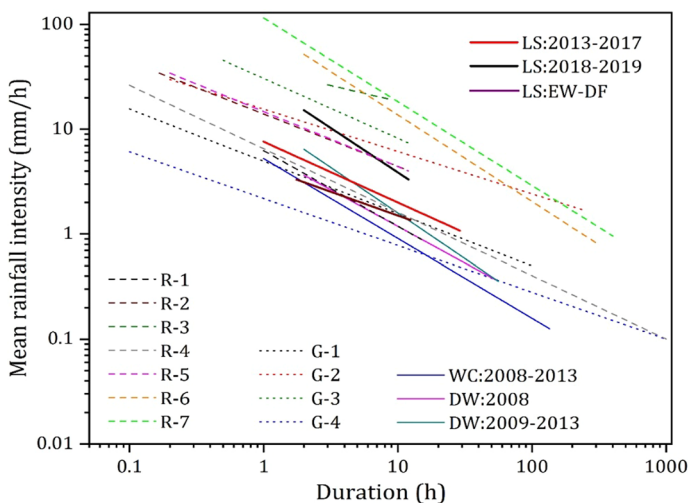


Fig. 14 Rainfall thresholds for debris flows in different time intervals

to their coexistence with other water-dominated flows (McGuire et al. 2017). As the initiation process was not monitored, the objectives of the study were to investigate the main material sources and the formation processes of massive debris flows. Nevertheless, field investigation revealed that the flows were of clear water only in the headwater regions. As the flows progressed, they were supplied by material from incision and lateral erosion processes and they turned into denser flows. Furthermore, some also developed through periodic blockage–breaking effects owing to the localized narrow topography typical of both studied watersheds. Although we found that the formation process at the watershed scale has a different meaning in comparison with the initiation process in headwater regions, the erosion phenomena observed were similar (e.g., Coe et al. 2008; Gregoretto and Dalla Fontana 2008; Kean et al. 2013; Degetto et al. 2015; Gregoretto et al. 2018; Simoni et al. 2020). The gullies were deep and incised laterally by runoff from low-permeability surfaces, and in local lower-gradient sections, narrow blockages acted as a “sediment capacitor” that helped amplify the flow discharge (Kean et al. 2013; Reid et al. 2016; McGuire et al. 2017; Tang et al. 2020).

The rainfall thresholds for the study area, which reflect the susceptibility to debris flows, were compared with other global and regional thresholds, especially those for the neighboring Wenchuan earthquake area (Fig. 15). First, debris flows in the study region are triggered by shorter-duration rainfall than in most other regions, including the Wenchuan earthquake area. Second, after the 2013 Lushan earthquake, the thresholds were lower than most other regional thresholds, except for the overall threshold for debris flows in Japan (Saito et al. 2010). However, they became higher than the global thresholds proposed by both Inners (1983) and Guzzetti (2008), and higher than the threshold proposed for the Wenchuan earthquake area (Guo et al. 2016a). Third, thresholds for the same time interval (1–5 years after the earthquake) were compared. The threshold line for the study area



**Fig. 15** Rainfall thresholds for debris flows in different regions. G-1: World (Inners, 1983); G-2: World (Caine 1980); G-3: World (Jibson 1989); G-4: World (Guzzetti et al. 2008); R-1: Jiangjia Ravine, Yunnan, China (Guo et al. 2020); R-2: South California, the USA (Cannon et al. 2008); R-3: Beijing, China (Ma et al. 2016); R-4: Japan (Saito et al. 2010); R-5: Central Italy (Guzzetti et al. 2007); R-6: Nepal, Himalaya (Dahal and Hasegawa 2008); R-7: Taiwan (Chen et al. 2005); DW: southwestern subregion of the Wenchuan earthquake area, close to the study area (Guo et al. 2016b, 2016c); WC: Wenchuan earthquake area (Guo et al. 2016a); EW-DF: debris flows supplied by engineering residue

in 2013–2017 intersects with that for the Du-Wen (D-W) region in 2009–2013. The D-W region, which is close to the study area, is one of the regions in the Wenchuan earthquake area most prone to the occurrence of debris flows (Guo et al. 2016a, b). However, the thresholds for 2018–2019 were much higher, indicating an obvious increasing tendency. Finally, the threshold for debris flows supplied by engineering residue is close to those proposed for debris flows in 2008 in the Wenchuan earthquake area, suggesting notably low inducing rainfall conditions.

Compared with the neighboring Wenchuan earthquake area (e.g., the D-W region), the debris-flow volumes were smaller, i.e., reported volumes were  $< 40 \times 10^4 \text{ m}^3$  and most were  $< 10 \times 10^4 \text{ m}^3$ . This is partially attributable to the smaller magnitude of the Lushan earthquake (Ms 7.0 vs 8.0) and to the humid climate that promotes vegetation recovery.

The increase of the rainfall thresholds can be attributed to two reasons: (1) natural recovery of the slopes, which suggests reduction of the quantity of movable solid material on the slopes and (2) the effect of debris-flow control projects. The climate in the study region is conducive to plant growth and vegetation recovered rapidly (i.e., within several years) following the earthquake. Furthermore, debris-flow control works consisting of check dams in gully headwaters and debris-flow dams in channels were initiated after the 2013 Lushan earthquake and completed in early 2014. These works resulted in substantial reduction of the frequency and magnitude of the debris in comparison with those of 2013 (Fig. 16). As shown in Fig. 17, control works were constructed in 27 gullies of the 47 potential debris-flows sites throughout the BXR basin. Of these, 11 had no debris flows during 2014–2018, and debris-flow volumes were effectively controlled in the other 16 gullies (Fig. 17). Nevertheless, debris flows remained significantly more active than before the 2008 earthquake. Taking the LMG as an example, field investigation suggested that  $> 250 \times 10^4 \text{ m}^3$  of loose material has been formed by slope failures and channel residue; however, no more than

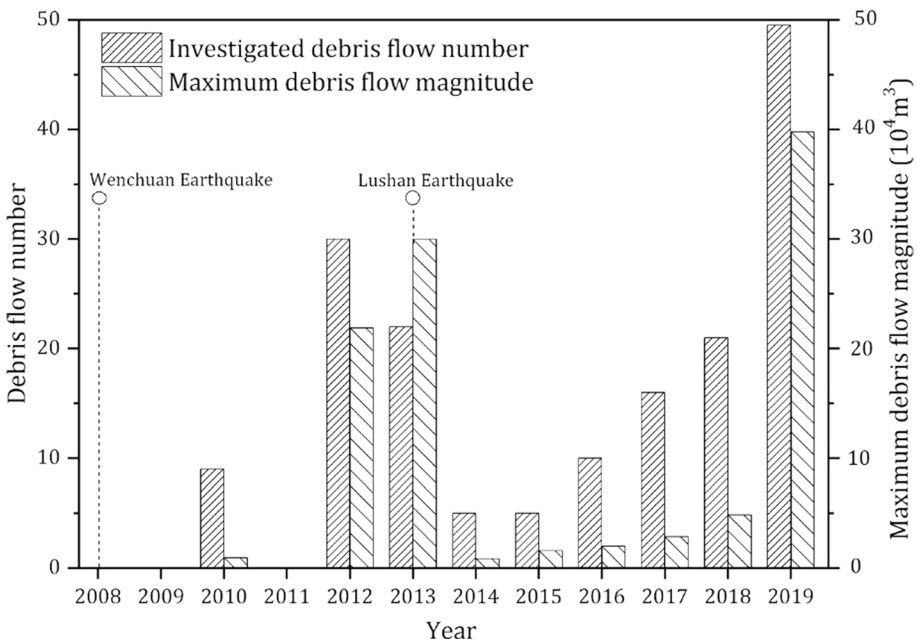
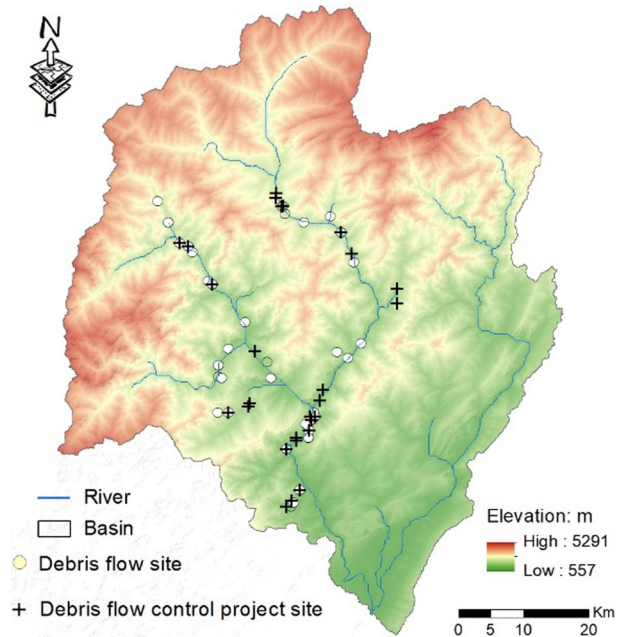


Fig. 16 Recorded debris-flow numbers and maximum debris-flow magnitudes (2010–2019)

**Fig. 17** Debris-flow control projects completed within the Baoxing River (BXR) basin since early 2014



$40 \times 10^4 \text{ m}^3$  has been released in the form of debris flows, indicating that 85% of this material remains erodible.

Human activities can both stimulate and suppress debris-flow activity. In the study area, poorly planned and/or executed engineering works (e.g., hydro stations, roads, and mining works) produce waste with which debris flows can be initiated more easily in comparison with natural slope/channel material (Figs. 9h and 11). Conversely, properly planned and executed control works can decrease the frequency of occurrence of debris flows and reduce the associated damage. Since 2014, fewer debris flows have been reported owing to the temporary effect of the check dams (Fig. 17). However, this effect has diminished over time owing to the decreasing capacities of the reservoirs, as reflected by the substantial damage that occurred in 2019 (Fig. 16).

## 6 Conclusions

In this work, the spatial distribution and formation processes of debris flows in the Lushan earthquake area of southwestern China were investigated; in addition, rainfall thresholds for debris-flow occurrence were proposed. Debris flows are mainly distributed in the northern part of the study area, which has a denser network of active faults. Rainfall is the triggering factor for debris-flow occurrence. The surface flow concentrates loose material, which then contributes to eroding further material along the channel bed, similar to the ‘progressive bulking’ effect. With further deep incision, lateral erosion, and blockage–breaking effects, the debris-flow magnitudes are amplified.

The rainfall conditions required vary for different-type debris-flows, in different regions, and also increased over time. Despite debris-flow control projects, the natural recovery of vegetation is an important factor for reducing debris flows. However, debris flows continue

to be active and have remained the most significant hazard in the region since the April 20 2013 Ms 7.0 Lushan earthquake. The results of this study provide a reference for debris-flow mitigation in earthquake-prone regions.

**Acknowledgements** This study was supported by the Second Qinghai-Tibet Plateau Scientific Research (2019QZKK0903-02), National Research and Development Program (2020YFC1512000 and 2017YFC1502504), NSFC (41977257), Department of Land and Resources Project of Sichuan Province (KJ-2018-22), and Western Light of Young Scholars, CAS. We thank James Buxton MSC from Liwen Bianji, Edanz Group China ([www.liwenbianji.cn/ac](http://www.liwenbianji.cn/ac)), for editing the English text of this manuscript.

## References

- Aleotti P (2004) A warning system for rainfall-induced shallow failures. *Eng Geol* 73:247–265
- Bardou E, Jaboyedoff M (2008) Debris flows as a factor of hillslope evolution controlled by a continuous or a pulse process? *Geol Soc Spec Publ* 296:63–78
- Berti M, Bernard M, Gregoretti C, Simoni A (2020) Physical interpretation of rainfall thresholds for runoff-generated debris flows. *Journal of Geophysical Research: Earth Surface*. <https://doi.org/10.1029/2019JF005513>
- Caine N (1980) The rainfall intensity–duration control of shallow landslides and debris flows. *Geografiska Annaler Series A Phys Geogr* 62:23–27
- Cannon SH, Bigio ER, Mine E (2001) A process for fire-related debris flow initiation, Cerro Grande fire, New Mexico. *Hydrol Process* 15(15):3011–3023
- Cannon S, Gartner J, Wilson R (2008) Storm rainfall conditions for floods and debris flows from recently burned areas in southwestern Colorado and southern California. *Geomorphology* 96:250–269
- Chang M, Tang C, Xia CH, Fang QS (2016) Spatial distribution analysis of landslides triggered by the 2013–04-20 Lushan earthquake, China. *Earthq Eng Eng Vib* 15:163–171
- Chen CY, Chen TC, Yu FC, Yu WH, Tseng CC (2005) Rainfall duration and debris-flow initiated studies for real-time monitoring. *Environ Geol* 47:715–724
- Chen CY (2016) Landslide and debris flow initiated characteristics after typhoon Morakot in Taiwan. *Landslides* 13:153–164
- Chen H, Petley DN (2005) The impact of landslides and debris flow triggered by typhoon Mindulle in Taiwan. *Q J Eng Geol Hydrogeol* 38:301–304
- Chen XL, Yu L, Wang MM, Lin CX, Liu CG, Li JY (2014) Brief communication: landslides triggered by the Ms =7.0 Lushan earthquake. *China Nat Hazards Earth Syst Sci*. 14(5):1257–1267
- Chen L, Wang H, Ran Y, Lei S, Li X, Wu F, Ma X, Liu C, Han F (2014) The 2013 Lushan Ms 7.0 earthquake: Varied seismogenic structure from the 2008 Wenchuan earthquake. *Seismol Res Lett* 85(1):34–39
- Coe JA, Kinner DA, Godt JW (2008) Initiation conditions for debris flows generated by runoff at Chalk Cliffs, central Colorado. *Geomorphology* 96(3–4):270–297
- Costa JE (1984) Physical geomorphology of debris flows. In: Costa JE, Fleischer PJ (eds) *Developments and Applications of Geomorphology*. Springer, Berlin, Germany, pp 268–317
- Cui P, Chen XQ, Zhu YY, Su FH, Wei FQ, Han YS, Liu HJ, Zhuang JQ (2011) The Wenchuan Earthquake (May 12, 2008), Sichuan Province, China, and resulting geohazards. *Nat Hazards* 56(1):19–36
- Cui P, Zhou GG, Zhu XH, Zhang JQ (2013) Scale amplification of natural debris flows caused by cascading landslide dam failures. *Geomorphology* 182:173–189
- Cui P, Zhang JQ, Yang ZJ, Chen XQ, You Y, Li Y (2014) Activity and distribution of geohazards induced by the Lushan earthquake, April 20, 2013. *Nat Hazards* 73:711–726
- Cui P, Guo XJ, Yan Y, Li Y, Ge YG (2018) Real-time observation of an active debris flow watershed in the Wenchuan Earthquake area. *Geomorphology* 321(15):153–166
- Degetto M, Gregoretti C, Bernard M (2015) Comparative analysis of the differences between using LiDAR contour based DEMs for hydrological modeling of runoff generating debris flows in the Dolomites. *Front Earth Sci* 3:21
- Domènech G, Fan XM, Scaringi G, van Asch TWJ, Xu Q, Huang RQ, Hales TC (2019) Modeling the role of material depletion, grain coarsening and revegetation in debris flow occurrences after the 2008 Wenchuan earthquake. *Eng Geol* 250:34–44
- Fan RL, Zhang LM, Wang HJ, Fan XM (2018) Evolution of debris flow activities in Gaojiagou Ravine during 2008–2016 after the Wenchuan earthquake. *Eng Geol* 235:1–10



- Fan X, Scaringi G, Korup O, West AJ, van Westen CJ, Tanyas H et al (2019) Earthquake-induced chains of geologic hazards: Patterns, mechanisms, and impacts. *Rev Geophysics* 57(2):421–503
- Gabet EJ, Bookter A (2008) A morphometric analysis of gullies scoured by post-fire progressively bulked debris flows in southwest Montana, USA. *Geomorphology* 96(3):298–309
- Godt JW, Coe JA (2007) Alpine debris flows triggered by a 28 July 1999 thunderstorm in the central Front Range. *Colorado Geomorphology* 84(1–2):80–97
- Griffiths PG, Webb RH, Melis TS (2004) Frequency and initiation of debris flows in Grand Canyon. *Arizona J Geophysical Res* 109:F04002
- Guo XJ, Cui P, Li Y, Ma L, Ge YG, William BM (2016a) Intensity-duration threshold of rainfall triggering debris flows in Wenchuan earthquake area, China. *Geomorphology* 263:208–216
- Guo XJ, Cui P, Li Y, Zhang JQ, Ma L, William BM (2016b) Spatial features of debris flows and their rainfall thresholds in the Wenchuan Earthquake-affected area. *Landslides* 13:1215–1229
- Guo XJ, Cui P, Li Y, Zou Q, Kong YD (2016c) The formation and development of debris flows in large watersheds after the 2008 Wenchuan Earthquake. *Landslides* 13:25–37
- Guo XJ, Cui P, Li Y, Fan JL, Yan Y, Ge YG (2016d) Temporal differentiation of rainfall thresholds for debris flows in Wenchuan earthquake-affected areas. *Environ Earth Sci* 75:1–12
- Gregoretti C, Fontana GD (2008) The triggering of debris flow due to channel-bed failure in some alpine headwater basins of the Dolomites: analyses of critical runoff. *Hydrol Process* 22:2248–2263
- Gregoretti C, Degetto M, Bernard M, Boreggio M (2018) The debris flow occurred at Ru Secco Creek, Venetian Dolomites, on 4 August 2015: analysis of the phenomenon, its characteristics and reproduction by models. *Frontier Earth Sci*. <https://doi.org/10.3389/feart.2018.00080>
- Guzzetti F, Peruccacci S, Rossi M, Stark C (2007) Rainfall thresholds for the initiation of landslides in central and southern Europe. *Meteorol Atmos Phys* 98:239–252
- Guzzetti F, Peruccacci S, Rossi M, Stark C (2008) The rainfall intensity–duration control of shallow landslides and debris flows: an update. *Landslides* 5:3–17
- Huang RQ, Li WL (2014) Post-earthquake landsliding and long-term impacts in the Wenchuan earthquake area. *China Eng Geol* 182:111–120
- Imaizumi F, Sidle RC, Tsuchiya S, Ohsaka O (2006) Hydrogeomorphic processes in a steep debris flow initiation zone. *Geophys Res Lett* 33:L10404
- Imaizumi F, Masui T, Yokota Y, Tsunetaka H, Hayakawa YS, Hotta N (2019) Initiation and runout characteristics of debris flow surges in Ohya landslide scar, Japan. *Geomorphology* 339:58–59
- Innes J (1983) Debris flows. *Prog Phys Geogr* 7:469–501
- Jibson R (1989) Debris flow in southern Puerto Rico. *Geol Soc Am Spec Pap* 236:29–55
- Li CR, Wang M, Liu K (2018) A decadal evolution of landslides and debris flows after the Wenchuan earthquake. *Geomorphology* 323:1–12
- Lin GW, Chen H, Chen YH, Horng MJ (2008) Influence of typhoons and earthquakes on rainfall-induced landslides and suspended sediments discharge. *Eng Geol* 97:32–41
- Lin CW, Shieh CL, Yuan BD, Liu SH, Lee SY (2003) Impact of Chi-Chi earthquake on the occurrence of landslides and debris flows: example from the Chenyulan River watershed, Nantou. *Taiwan Eng Geol* 71:49–61
- Lin CW, Liu SH, Lee SY, Liu CC (2006) Impacts of the Chi-Chi earthquake on subsequent rainfall-induced landslides in central Taiwan. *Eng Geol* 86:87–101
- Kean JW, McCoy SW, Tucker GE, Staley DM, Coe JA (2013) Runoff-generated debris flows: Observations and modeling of surge initiation, magnitude, and frequency. *J Geophysical Res: Earth Surf* 118(4):2190–2207
- Koch T (1998) Testing of various constitutive equations for debris flow modelling. In: Kovar K et al (eds) *Hydrology, Water Resources and Ecology in Headwaters*, IAHS Publ No 248. Merano, Italy, pp 249–257
- Ma C, Wang YJ, Hu KH, Du C, Yang WT (2017) Rainfall intensity–duration threshold and erosion competence of debris flows in four areas affected by the 2008 Wenchuan earthquake. *Geomorphology* 282:85–95
- Ma C, Deng J, Wang R (2018) Analysis of the triggering conditions and erosion of a runoff-triggered debris flow in Miyun County, Beijing, China. *Landslides* 15:2475–2485
- McGuire LA, Rengers FK, Kean JW, Staley DM (2017) Debris flow initiation by runoff in a recently burned basin: Is grain-by-grain sediment bulking or en-masse failure to blame? *Geophys Res Lett*. <https://doi.org/10.1002/2017GL074243>
- Ouyang CJ, He SM, Tang C (2015) Numerical analysis of dynamics of debris flow over erodible beds in Wenchuan earthquake-induced area. *Eng Geol* 194:62–72

- Prenner D, Kaitna R, Mostbauer K, Hrachowitz M (2018) The Value of Using Multiple Hydrometeorological Variables to Predict Temporal Debris Flow Susceptibility in an Alpine Environment. *Water Resour Res* 54(9):6822–6843
- Prenner D, Hrachowitz M, Kaitna R (2019) Trigger characteristics of torrential flows from high to low alpine regions in Austria. *Sci Total Environ* 658:958–972
- Reid ME, Coe JA, Brien DL (2016) Forecasting inundation from debris flows that grow volumetrically during travel, with application to the Oregon Coast Range, USA. *Geomorphology* 273:396–411
- Rickenmann D (1999) Empirical relationships for debris flows. *Nat Hazards* 19(1):47–77
- Saito S, Daichi N, Hiroshi M (2010) Relationship between the initiation of a shallow landslide and rainfall intensity-duration thresholds in Japan. *Geomorphology* 118:1125–1175
- Shieh C, Chen Y, Tsai Y, Wu JH (2009) Variability in rainfall threshold for debris flow after the Chi-Chi earthquake in central Taiwan, China. *Int J Sedim Res* 24:177–188
- Simoni A, Bernard M, Berti A, Boreggio M, Lanzoni S, Stancanelli L, Gregoret C (2020) Runoff-generated debris flows: observation of initiation conditions and erosion-deposition dynamics along the channel at Cancia (eastern Italian Alps). *Earth Surf Proc Land*. <https://doi.org/10.1002/esp.4981>
- Smith HG, Sheridan GJ, Nyman P, Child DP, Lane PN, Hotchkis MA, Jacobsen GE (2012) Quantifying sources of ne sediment supplied to post-fire debris flows using fallout radionuclide tracers. *Geomorphology* 139:403–415
- Shou KJ, Wu CC, Fei LY, Lee JF, Wei CY (2011) Dynamic environment in the Ta-Chia River watershed after the 1999 Taiwan. Chi-Chi earthquake *Geomorphology* 133:190–198
- Tang C, Ma GC, Chang M, Li WL, Zhang DD, Jia T, Zhou ZY (2015) Landslides triggered by the 20 April 2013 Lushan earthquake, Sichuan Province, China. *Eng Geol* 187:45–55
- Tang H, McGuire L, Kean J, Smith J (2020) The impact of sediment supply on the initiation and magnitude of runoff-generated debris flows. *Geophys Res Lett*. <https://doi.org/10.1029/2020GL087643>
- Wang CD, Xie J (2018) The formation mechanism and characteristics of debris flows in Lengmu Gully on 2012.8.18. Shaanxi Shuili 6:61–63 (in Chinese)
- Wang E, Meng Q (2009) Mesozoic and Cenozoic tectonic evolution of the Longmenshan fault belt. *Sci China Ser D Earth Sci* 52:579–592
- Xu C, Xu XW, Bruce J, Shyu H (2015) Database and spatial distribution of landslides triggered by the Lushan, China Mw 6.6 earthquake of 20 April 2013. *Geomorphology* 248:77–92
- Yin YP, Wang FW, Sun P (2009) Landslide hazards triggered by the 2008 Wenchuan earthquake, Sichuan. *China Landslides* 6(2):139–152
- Zhang Y, Dong S, Hou C, Guo C, Yao X, Li B, Du J, Zhang J (2013) Geohazards induced by the Lushan Ms 7.0 earthquake in Sichuan Province, southwest China: typical examples, types and distributional characteristics. *Acta Geol Sin* 87:646–657
- Zhang S, Zhang LM (2017) Impact of the 2008 Wenchuan earthquake in China on subsequent long-term debris flow activities in the epicentral area. *Geomorphology* 276:86–103
- Zhou W, Tang C (2014) Rainfall thresholds for debris flow initiation in the Wenchuan earthquake-stricken area, southwestern China. *Landslides* 11(5):877–887